Available online at www.sciencedirect.com
ScienceDirect
Journal of Power Sources 162 (2006) 1367–1372
JOURNAL OF POWER SOURCES
www.elsevier.com/locate/jpowsour

Short communication

Synthesis and electrochemical properties of Mo-doped $Li[Ni_{1/3}Mn_{1/3}Co_{1/3}]O_2$ cathode materials for Li-ion battery

Li Qin Wang, Li Fang Jiao, HuaTang Yuan *, Jian Guo, Ming Zhao, Hai Xia Li, Yong Mei Wang

Institute of New Energy Material Chemistry, Nankai University, Tianjin 300071, China

Received 29 March 2006; received in revised form 29 August 2006; accepted 30 August 2006
Available online 9 October 2006

Abstract

The layered $Li[Ni_{(1-x)/3}Mn_{(1-x)/3}Co_{(1-x)/3}Mo_x]O_2$ cathode materials ($x = 0$, 0.005, 0.01, and 0.02) were prepared by a solid-state pyrolysis method (700, 800, 850, and 900 °C). Its structure and electrochemical properties were characterized by XRD, SEM, XPS, cyclic voltammetry, and charge/discharge tests. It can be learned that the doped sample of $x = 0.01$ calcined at 800 °C shows the highest first discharge capacity of 221.6 mAh g^{-1} at a current density of 20 mA g^{-1} in the voltage range of 2.3–4.6 V, and the Mo-doped samples exhibit higher discharge capacity and better cycle-ability than the undoped one at room temperature.
© 2006 Elsevier B.V. All rights reserved.

Keywords: Li-ion battery; MoO_3; Doping; Cathode material

1. Introduction

Rechargeable lithium-ion batteries are becoming increasingly important as power sources for portable consumer electronics. $LiCoO_2$, which has been commercially used as a cathode material for Li-ion batteries, shows a stable discharge capacity. However, due to its high cost and toxicity, many efforts have been made to replace it.

Recently, intensive effort has been directed towards the development of $LiNi_xCo_yMn_{1-y}O_2$ [1–6], especially for $Li[Ni_{1/3}Mn_{1/3}Co_{1/3}]O_2$. It has a typical hexagonal α-$NaFeO_2$ structure with a space group of *R*-3*m*. Layer-structured $Li[Ni_{1/3}Mn_{1/3}Co_{1/3}]O_2$ has shown to be the most promising alternative material in terms of operating voltage, capacity, cycle-ability, thermal stability, and material cost [7–10]. However, it has many problems as well, such as low rate capability and tap density, which should be resolved before it can be replaced $LiCoO_2$. The inferior rate capability arises from the low electronic conductivity of $Li[Ni_{1/3}Mn_{1/3}Co_{1/3}]O_2$ [11].

There are two methods to improve the electrochemical performance, one is to modify the surface properties of the cathode materials by coating particles with metal oxide (ZnO, Al_2O_3, ZrO_2, TiO_2, and SiO_2 [12–15]) to prevent dissolution of transition metals and unwanted reactions between cathode and electrolyte [11]; the other is to partially substitute manganese, cobalt, and nickel ions for transition metals, such as iron, titanium, molybdenum, or chromium and non-transition metals, such as aluminum or magnesium, which may stabilize the layered structure with or without participating in the redox processes and prevent unwanted reactions between cathode and electrolyte. However, to the best of our knowledge, no studies on the electrochemical performance of electrode-active materials doped by molybdenum ions have been published.

In this study, we employed Mo as an additional dopant to synthesize a series of Mo-doped $Li[Ni_{(1-x)/3}Mn_{(1-x)/3}Co_{(1-x)/3}Mo_x]O_2$ ($x = 0$, 0.005, 0.01, and 0.02) powders by a solid-state pyrolysis reaction. The structural, morphological and electrochemical performance of the layered $Li[Ni_{(1-x)/3}Mn_{(1-x)/3}Co_{(1-x)/3}Mo_x]O_2$ powders were studied in this paper.

2. Experimental

2.1. Synthesis of $Li[Ni_{(1-x)/3}Mn_{(1-x)/3}Co_{(1-x)/3}Mo_x]O_2$ powders

$Li[Ni_{(1-x)/3}Mn_{(1-x)/3}Co_{(1-x)/3}Mo_x]O_2$ ($x = 0$, 0.005, 0.01, and 0.02) powders were prepared as follows: stoichiometric

* Corresponding author. Tel.: +86 22 23498089; fax: +86 22 23502604.
E-mail addresses: yufan@mail.nankai.edu.cn (L.Q. Wang), yuanht@nankai.edu.cn (H. Yuan).

0378-7753/$ – see front matter © 2006 Elsevier B.V. All rights reserved.
doi:10.1016/j.jpowsour.2006.08.033

$LiCH_3COO{\cdot}2H_2O$, $Ni(CH_3COO)_2{\cdot}4H_2O$, $Mn(CH_3COO)_2{\cdot}4H_2O$, $Co(CH_3COO)_2{\cdot}4H_2O$ (cationic molar ratio of Li:Ni:Mn:Co = 1.1:(1 − x)/3:(1 − x)/3:(1 − x)/3) were used as the starting materials. These reagents were mixed, thoroughly ground and then added MoO_3 with atomic ratio Mo/(Mn + Ni + Co + Mo) = 0, 0.005, 0.01, and 0.02. The mixtures were heated at 120 °C for 48 h to obtain the precursors. Precursors were thoroughly ground again and then the powder mixture was pressed under 30 MPa pressure into a small pellet and calcined at 750, 800, 850, and 900 °C for 20 h in air, respectively.

2.2. Measurements

X-ray diffraction measurements of the as-prepared $Li[Ni_{(1-x)/3}Mn_{(1-x)/3}Co_{(1-x)/3}Mo_x]O_2$ materials were carried out using X-ray diffraction (D/Max-2500) with Cu Kα radiation at room temperature. Particle morphology of the powders after calcination was observed using a scanning electron microscope (SEM, JSM 6400, JEOL, Japan).

Power X-ray photoelectron spectra (XPS)(AXIS ULTRA DLD produced by Kratos company & Shimadu company, with monochromatic Mg Kα radiation ($h\nu$ = 1253.6 eV)) was done to determine the valence of Mo. Charge reference was done against the binging energy (BE) of adventitious carbon (C 1s = 284.6 eV). The spectra was analysed using the XPS Peak fit software.

The composite positive electrodes were prepared by pressing a mixture of the active materials, conductive material (acetylene black) and binder (PTFE) in a weight ratio of 85/10/5. The Li metal was used as the counter and reference electrodes. The electrolyte was 1 M $LiPF_6$ in a 6/3/1 (volume ratio) mixture of ethylene carbonate (EC), propylene carbonate (PC), and dimethyl carbonate (DMC). The cells were assembled in an argon-filled dried box. Charge–discharge tests were performed between 2.3 and 4.6 V. Cyclic voltammetry experiments were performed by using a CHI660 Electrochemical Workstation at a scan rate of 0.1 mV s^{-1}. All tests were performed at room temperature.

3. Results and discussion

3.1. The influence of calcined temperature on the structure and particle size of the doped samples

Fig. 1 illustrates the typical XRD patterns of the synthesized $Li[Ni_{0.33}Mn_{0.33}Co_{0.33}Mo_{0.01}]O_2$ materials calcined at different temperatures of 750, 800, 850, and 900 °C, respectively. Hereafter, the materials synthesized at 750, 800, 850, and 900 °C were referred as S75, S80, S85, and S90. As shown in Fig. 1, all peaks are sharp and well-defined, suggesting that the compounds are generally well crystallized. All the samples can be indexed on the basis of the α-$NaFeO_2$ structure (space group: 166, *R*-3*m*). While impurity phases (a sawtooth peak between 20° and 23°) like Li_2MnO_3 are observed for S85. The crystal structure of Li_2MnO_3 consists of cubic close-packed oxide ion layers with alternate sheets

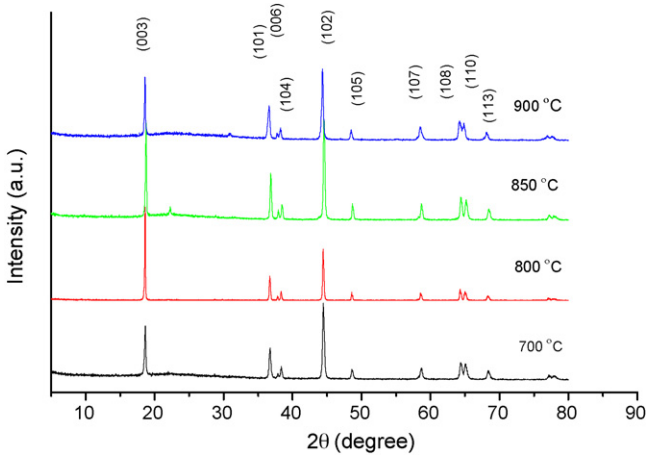

Fig. 1. XRD patterns of $Li[Ni_{0.33}Mn_{0.33}Co_{0.33}Mo_{0.01}]O_2$ samples calcined at different temperatures.

of octahedral sites occupied by Li and $[Li_{1/3}Mn_{2/3}]$ [16]. As can be seen in Fig. 1, regardless of low calcination temperature, the peak splits of (0 0 6)/(1 0 2) and (1 0 8)/(1 1 0) are observed in all the XRD patterns, indicating that the layered $Li[Ni_{0.33}Mn_{0.33}Co_{0.33}Mo_{0.01}]O_2$ cathode material has been synthesized successfully at all the calcination temperature in this experiment.

The intensity ratio of I_{003}/I_{104} which was reported to be sensitive to the degree of cation mixing in lattice and electrochemical properties of the material [17] was summarized in Table 1. The values of S75 and S90 are smaller than 1, indicating that some cation mixing takes place. While the values of S80 and S85 are larger than 1, suggesting that no undesirable cation mixing takes place. As mentioned above, it can be concluded that the calcined temperature has a significant influence on the sample structure, which may lead to the distinct difference in the electrochemical capability.

In order to further study, the influence of the calcination temperature on the structure and particle size of samples, SEM observation was operated. Fig. 2 reveals micro morphologies of all samples. The thermal decomposition of precursor at 750 °C results in the primary formation of smaller than 1 μm crystallites of $Li[Ni_{0.33}Mn_{0.33}Co_{0.33}Mo_{0.01}]O_2$. Meanwhile some greater agglomerations should exhibit that not all the raw materials had reacted absolutely. With increasing the calcination temperature, the primary particles increase. The particle size of S80 ranges from 2 to 3 μm, nearly twice as large as that of S75. The morphology has better-shaped, smoother crystals with sharper edges. When the temperature reaches 900 °C, the morphology of the sample is obviously particle-agglomerated, and the primary particle size is more than 6 μm, which might cause the electrochemical capability descend distinctly. From all mentioned

Table 1
I_{003}/I_{104} of $Li[Ni_{0.33}Mn_{0.33}Co_{0.33}Mo_{0.01}]O_2$ samples calcined at different temperatures

Calcined temperature (°C)	750	800	850	900
I_{003}/I_{104}	0.67	1.79	1.12	0.80

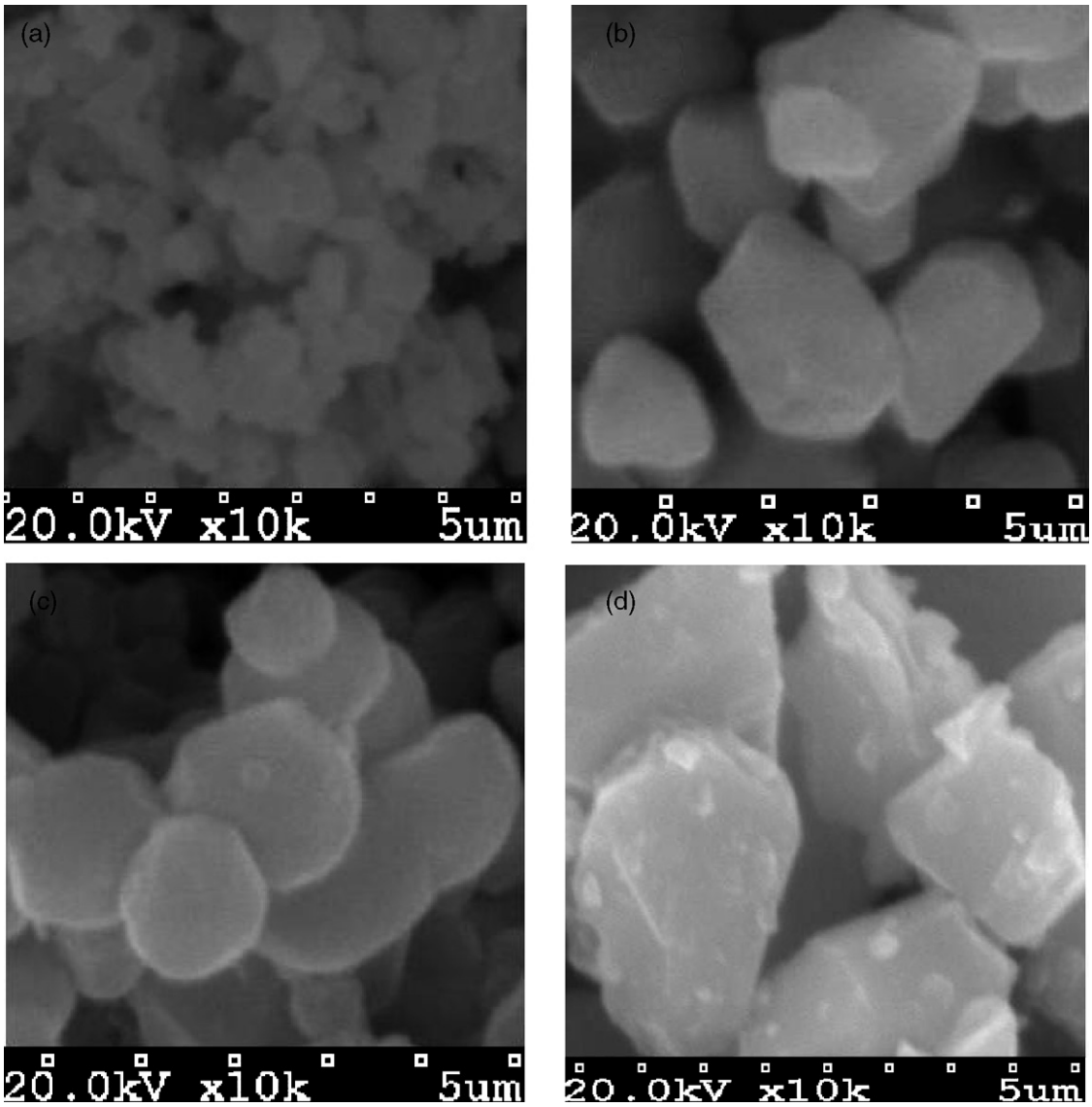

Fig. 2. SEM images of $Li[Ni_{0.33}Mn_{0.33}Co_{0.33}Mo_{0.01}]O_2$ synthesized at 750 °C (a), 800 °C (b), 850 °C (c), and 900 °C (d).

above, it could be considered that 800 °C is the best synthetic temperature.

3.2. Properties of different Mo-doped samples

Fig. 3 shows the results of XRD studies for the synthesized $Li[Ni_{(1-x)/3}Mn_{(1-x)/3}Co_{(1-x)/3}Mo_x]O_2$ ($x = 0$, 0.005, 0.01, and 0.02) materials at 800 °C. The XRD patterns of all materials could be indexed based on the α-$NaFeO_2$ structure (space group: 166, *R*-3*m*). We could not observe any impurity in the measured range and all samples showed the integrated peak splits of (0 0 6)/(1 0 2) and (1 0 8)/(1 1 0) implying that a partly molybdenum substitution for manganese, cobalt, and nickel in $Li[Ni_{(1-x)/3}Mn_{(1-x)/3}Co_{(1-x)/3}Mo_x]O_2$ compounds has not changed the bulk structure of the pristine material.

The determined parameters are summarized in Table 2. With the increase of molybdenum content, the I_{003}/I_{104} peak intensity ratio is 1.07, 1.56, 1.78, and 1.61, indicating that over much

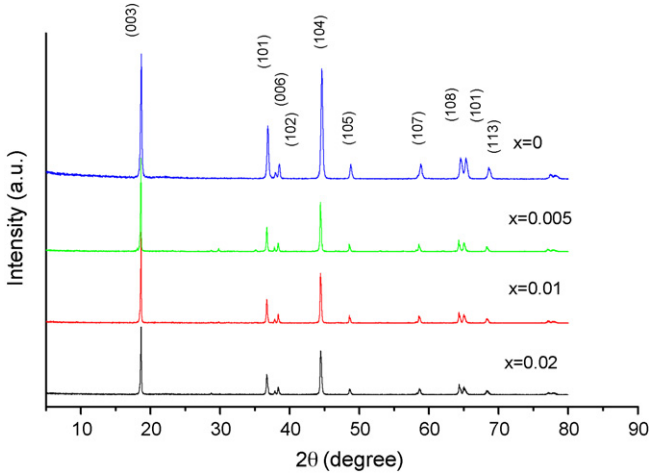

Fig. 3. XRD patterns of $Li[Ni_{(1-x)/3}Mn_{(1-x)/3}Co_{(1-x)/3}Mo_x]O_2$ ($x = 0$, 0.005, 0.01, and 0.02) samples.

Table 2
Chemical analysis lattice parameters of $Li[Ni_{(1-x)/3}Mn_{(1-x)/3}Co_{(1-x)/3}Mo_x]O_2$ materials synthesized at 800 °C

Samples	a (Å)	c (Å)	c/a	V(Å^3)	I_{003}/I_{104}	Specific surface area (m^2 g^{-1})
$X=0$	2.8496	14.2045	4.98	100.89	1.07	8.3
$X=0.005$	2.8671	14.2443	4.97	101.41	1.56	9.1
$X=0.01$	2.8684	14.2547	4.97	101.57	1.79	12.6
$X=0.02$	2.8671	14.2689	4.98	101.58	1.61	8.5

amount of molybdenum substitution should have a distinct influence on the sample structure. Among the samples, the I_{003}/I_{104} peak intensity ratio of $x=0.01$ is the highest, which might suggest that it has the best electrochemical properties.

The data of Table 2 show that a, c parameter and the unit cell volume somewhat increase with increasing Mo content x. It may be attributed to that in the same oxidation state molybdenum ions ($r^{6+}_{Mo}=0.62$ Å) are smaller than manganese ($r^{3+}_{Mn}=0.68$ Å) ions but bigger than cobalt ions ($r^{3+}_{Co}=0.545$ Å) and nickel ions ($r^{3+}_{Ni}=0.56$ Å) in size. While c/a ratio which indicates hexagonal structure disorder is virtually unchanged. It can be concluded that the specific surface area increases but hexagonal ordering does not change with increasing Mo-doped contents. Furthermore, a partly substituted Mo weakens the ordering degree of layered structure.

Mo XPS core spectra for discharged-$Li[Ni_{0.33}Mn_{0.33}Co_{0.33}Mo_{0.01}]O_2$ material is showed in Fig. 4. The Mo spectra appears complicated, which can be deconvoluted into four well-defined contributions. The four peaks, centred at 235.6, 232.3, 233.9, and 230.7 eV, correspond to Mo^{6+} (3d3/2), Mo^{6+} (3d5/2), Mo^{4+} (3d3/2), and Mo^{4+} (3d5/2) [18–21], respectively. It reveals that the Mo^{6+} ions are partly changed into Mo^{4+} ions after the material discharged. The data suggest that the doped samples clearly exhibit enhanced capacity during cycling, not only because the doped samples allows Li^+ ions to be extracted more [22], but also because the reduction of Mo^{6+} to Mo^{4+} increases the resulting capacity.

Fig. 5 compares the cyclic voltammograms of the $Li[Ni_{(1-x)/3}Mn_{(1-x)/3}Co_{(1-x)/3}Mo_x]O_2$ ($x=0$, 0.005, 0.01, and 0.02) samples obtained at a scan rate of 0.1 mV s^{-1}, between 2.3 and 4.6 V at room temperature. As shown, the intensity of anodic peaks shows much more increase than that of cathodic peaks as the value of x increased from 0 to 0.02. It indicates that the initial discharge capacity of Mo-doped samples are higher than that of pristine material with less irreversible capacity, then the coulombic efficiency of the electrode also increases. When $x=0$, anodic peak is observed at about 4.0 V during the first charge. The main oxidation peak (anodic peak) of all Mo-doped samples slightly shift to lower voltage about 3.7–3.8 V. It has been well known that Ni^{2+}/Ni^{4+} coupling is electrochemical redox process in the 3.6–3.8 V for $Li[Ni_{1/3}Mn_{1/3}Co_{1/3}]O_2$ systems.

It can be concluded that the polarization of samples decreases along with the increase of molybdenum amount, which probably due to the decreasing in cell resistant. The data in Table 2 show that the samples with higher Mo-doped contents have larger specific surface area, leading to less cell resistant. These observations suggest that Mo substitution induces some structural ordering or a reduction of stacking faults during the first Li de-intercalation in the case of $Li[Ni_{(1-x)/3}Mn_{(1-x)/3}Co_{(1-x)/3}Mo_x]O_2$ [23], resulting in the increase of the first specific discharge capacity and coulombic efficiency of the electrode.

Fig. 6 compares the initial charge–discharge curves of the $Li[Ni_{(1-x)/3}Mn_{(1-x)/3}Co_{(1-x)/3}Mo_x]O_2$ ($x=0$, 0.005, 0.01, and 0.02) with current density of 20 mA g^{-1} between 2.3 and 4.6 V at room temperature. The cell voltage of the samples rapidly increases to about 3.7 V and then holds at about 3.7–3.8 V at which Ohzuku and co-workers [24] reported the oxidation of Ni^{2+} to Ni^{3+} occurred. Moreover, the electrodes composed of Mo-doped samples show longer voltage plateaus and higher discharge voltage plateaus than the pristine material,

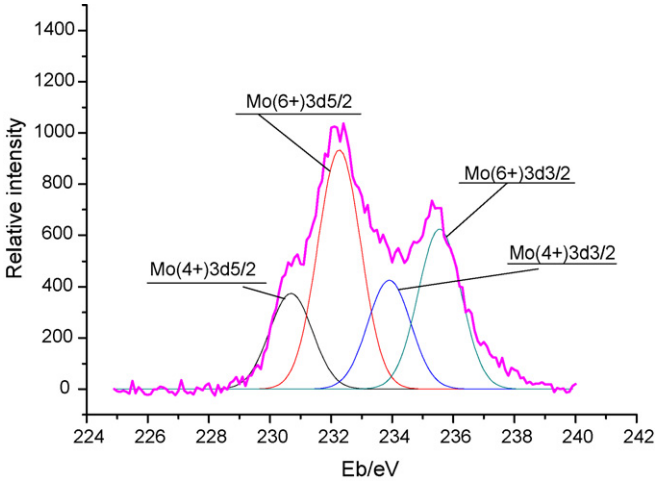

Fig. 4. XPS spectra of Mo of discharged-$Li[Ni_{0.33}Mn_{0.33}Co_{0.33}Mo_{0.01}]O_2$.

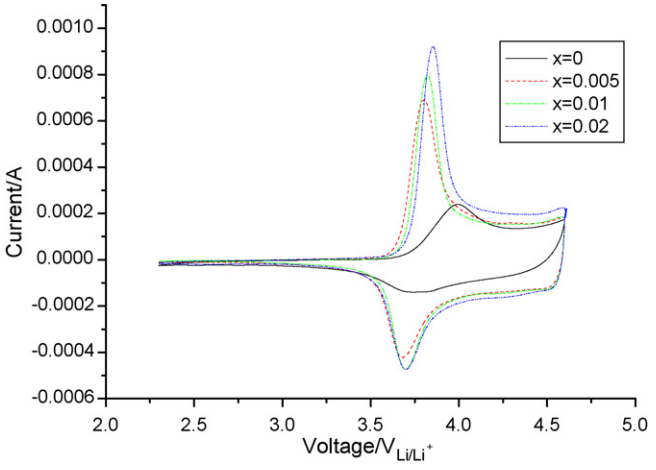

Fig. 5. Cyclic voltammogram of samples doped and undoped with Mo.

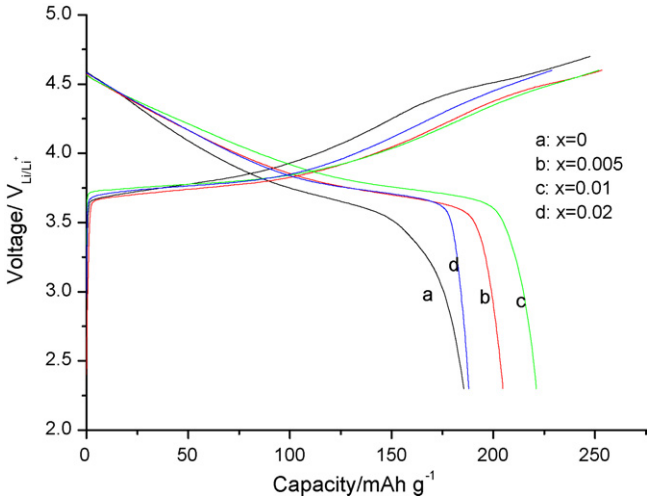

Fig. 6. Initial charge and discharge curves of different doped samples.

illuminating that a partly substituted molybdenum samples have lower resistance, and could deliver a higher specific discharge capacity.

Fig. 7 compares cycle stability of four samples at room temperature. As shown in Fig. 7, all of the Mo-doped samples deliver better cyclic performance and higher initial discharge capacity. The highest initial discharge capacity of 221.6 mAh g^{-1} together with the best cyclic performance is obtained at $x = 0.01$. And after 50 cycles, its discharge capacity is 185.9 mAh g^{-1}, and it has a least irreversible capacity loss of 16.1%. Therefore, the appropriate doping of molybdenum could give more advantage than surface area and lithium content. It also can be concluded that the proper doping of molybdenum can exert significant influence on the structure of these samples, which could affect the electrochemical performance.

In order to investigate the rate capability of the $Li[Ni_{(1-x)/3}Mn_{(1-x)/3}Co_{(1-x)/3}Mo_x]O_2$ ($x = 0$, 0.01, and 0.02), we applied various current densities of 30, 60, 120, 240, and 360 mA g^{-1} for charge–discharge in the voltage range of 2.3–4.6 V. As shown in Fig. 8, when $x = 0.01$, electrode exhibits a higher discharge

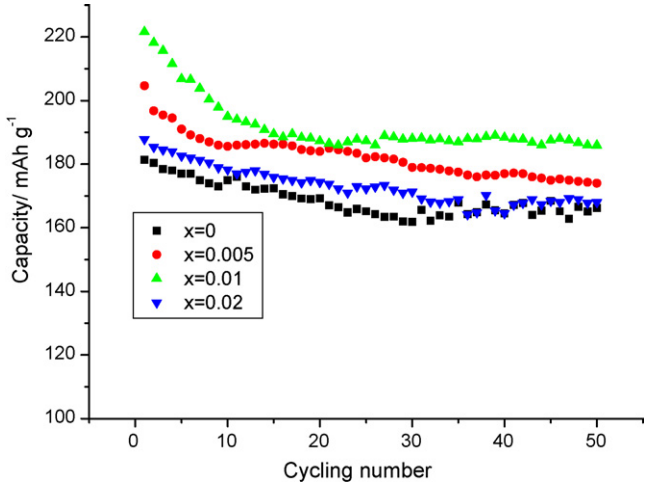

Fig. 7. Cycling performances of different Mo-doped samples.

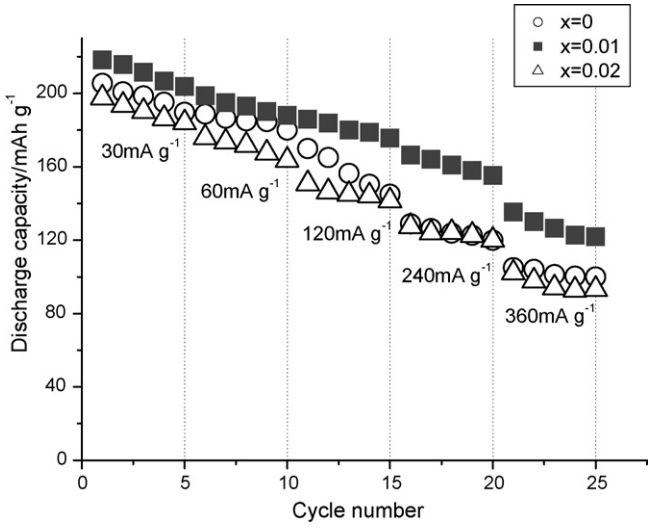

Fig. 8. The capacity retention of $Li/Li[Ni_{(1-x)/3}Mn_{(1-x)/3}Co_{(1-x)/3}Mo_x]O_2$ ($x = 0$, 0.01, and 0.02) cells during cycling at various rates in the voltage range of 2.3–4.6 V at room temperature.

capacity and better cycle-ability than that of the other electrodes at each current rate. The data thus demonstrate that the proper molybdenum substitution improves the cycle stability of the cathode materials at high rates. The best rate capability of sample of $x = 0.01$ than that of other samples is due to its small particle size and large specific surface.

4. Conclusion

The layered $Li[Ni_{(1-x)/3}Mn_{(1-x)/3}Co_{(1-x)/3}Mo_x]O_2$ ($x = 0$, 0.005, 0.01, and 0.02) cathodes have been synthesized by solid-state pyrolysis method at different temperatures (750, 800, 850, and 900 °C). The difference in various amounts of molybdenum substitution and calcined temperatures results in different morphology (shape, particle size, and specific surface area) and thereby different initial discharge capacity and the circular stability. Based upon the results of the electrochemical experiments, we can find that the ideal synthesized condition was 800 °C and the best amount of Mo substitution was $x = 0.01$. It shows the highest first discharge capacity of 221.6 mAh g^{-1} (2.3–4.6 V, 20 mA g^{-1}) and the smallest irreversible capacity loss of 16.1%. Besides, it has better cycle-ability at high current densities at room temperature.

Acknowledgements

This work was supported by TSTC(06YFJMC04900) and "TianJin-NanKai Union Fund", China.

References

[1] Y. Chen, G.X. Wang, J. Power Sources 119 (2003) 184.
[2] J.M. Kim, H.-T. Chung, Electrochim. Acta 49 (2004) 3573.
[3] N. Tran, Solid State Ionics 176 (2005) 1539.
[4] H. Cao, Y. Zhang, Solid State Ionics 176 (2005) 1207.
[5] H.-S. Shin, H.-S. Park, Solid State Ionics 176 (2005) 2577.
[6] J. Guo, L.F. Jiao, H.T. Yuan, Electrochim. Acta 51 (2006) 3731.

[7] Z. Lu, D.D. MacNeil, J.R. Dahn, Electrochem. Solid-State Lett. 4 (2001) 191.
[8] T. Ohzuku, Y. Makimura, Chem. Lett. 30 (2001) 642.
[9] I. Belharouak, Y.-K. Sun, J. Liu, K. Ammine, J. Power Sources 123 (2003) 247.
[10] S.H. Park, C.S. Yoon, H.-S. Kim, S.-I. Moon, Y.-K. Sun, Electrochim. Acta 49 (2004) 557.
[11] S.B. Jang, S.-H. Kang, K. Amine, Y.C. Bae, Y.-K. Sun, Electrochim. Acta 50 (2005) 4168.
[12] Y.-K. Sun, Y.-S. Lee, M. Yoshio, K. Amine, Electrochem. Solid-State Lett. 5 (2002) 99.
[13] J. Cho, Y.J. Kim, B. Park, Chem. Mater. 12 (2000) 3788.
[14] J. Cho, T.-J. Kim, B. Park, Electrochem. Solid-State Lett. 4 (2001) 159.
[15] A. Chobelt, H.C. Shiao, H.-P. Lin, M. Salomon, V. Manivannan, Electrochem. Solid-State Lett. 4 (2001) A65.
[16] P. Strobel, B. Lambert-Andron, J. Solid State Chem. 75 (2003) 90.
[17] T. Ohzuku, A. Ueda, M. Nagayama, J. Electrochem. Soc. 140 (1993) 1862.
[18] M. Shimoda, T. Hirata, K. Yagisawa, M. Okochi, A. Yoshikawa, J. Mater. Sci. Lett. 8 (1989) 1089.
[19] K.S. Kim, W.E. Baitinger, J.W. Amy, N. Winograd, J. Electron Spectrosc. Relat. Phenom. 5 (1974) 351.
[20] B. Brox, I. Olefjord, Surf. Interface Anal. 13 (1988) 3.
[21] W.E. Swartz, D.M. Hercules, Anal. Chem. 43 (1971) 1774.
[22] S.-H. Park, S.W. Oh, Y.-K. Sun, J. Power Sources 146 (2005) 622.
[23] X.l. Wu, K.S. Ryu, Y.-S. Hong, J. Power Sources 132 (2004) 219.
[24] Y. Koyama, I. Tanaka, H. Adachi, Y. Makimura, T. Ohzuku, J. Power Sources 119–121 (2003) 644.